Evaluation of Pt-Au/MWCNT (Multiwalled Carbon Nanotubes) electrocatalyst performance as cathode of a proton exchange membrane fuel cell

Mara Beltrán Gastélum[1], M. I. Salazar Gastélum[1], Rosa María Félix Navarro[1], S. Pérez Sicairos[1], E. A. Reynoso Soto[1], S. W. Lin[1], José Roberto Flores Hernández[2], Tatiana Romero Castañón[2], Irma Lorena Albarrán Sánchez[2] and F. Paraguay Delgado[3]

Article originally published in Energy 109 (2016) 446-455, ELSEVIER

[1] Centro de Graduados e Investigación en Química, Instituto Tecnológico de Tijuana
[2] Instituto Nacional de Electricidad y Energías Limpias
[3] Centro de Investigación en Materiales Avanzados SC

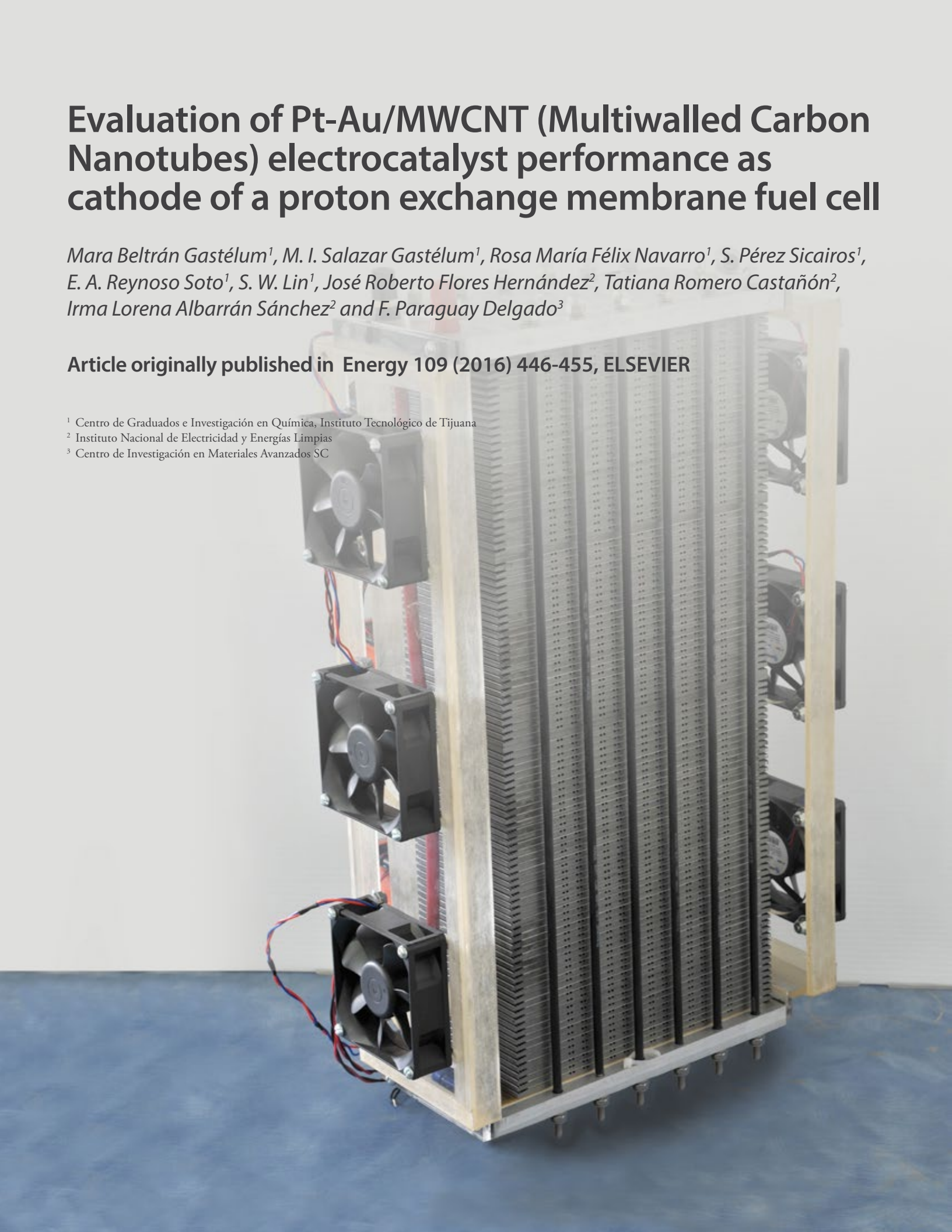

Abstract

A comparative study between Pt-Au/MWCNT and Pt/C (commercial) as cathodic electrocatalyst of H_2/O_2 fuel cell is performed. Pt-Au/MWCNT is synthesized using the reverse microemulsion method and this procedure is scaled-up in order to prepare membrane-electrode assemblies for fuel cells with an active area of 9 cm^2. Those electrocatalysts are characterized by both physicochemical techniques and electrochemical measurements to evaluate their catalytic activity for Oxygen Reduction Reaction (ORR). In the half-cell study, Pt-Au/MWCNT show higher kinetic current density as cathodic electrocatalyst compared with Pt/C. Likewise, in a fuel cell hardware the maximum power density is significantly higher for Pt-Au/MWCNT cathode (625 mW cm^{-2} at 0.426 V) when compared with Pt/C anode (355 mW cm^{-2} at 0.499 V).

1. Introduction

One of the main concerns of the last decades has been the demand for efficient energy sources to supply energetic requirements worldwide [1]. Energy sources based on petroleum and hydrocarbon are the most employed to satisfy the population energetic demand [2]. Nevertheless, two main adverse effects are implied: (a) Petroleum is limited and it is anticipated that the availability of this source will decrease [3]; (b) Most hydrocarbons contribute significantly to pollution generation, increasing the concentration of the greenhouse effect gases. Furthermore, gases such as NO_x and SO_x are also involved either in oil refinery or energy generation process from hydrocarbon sources [4].

Hence, new sustainable energy sources such as solar [5], wind [6], geothermal [7], hydro [8] have emerged as an alternative to supply the energetic requirements of the mankind and have gained importance in recent years. Renewable energies have the advantage of producing clean energy on site, but lack the capability to produce steady power as the resource will vary according to the weather conditions. Batteries, capacitors and fuel cells are ideal companions to renewable energies and can complement these technologies as they supply electricity during intermittent energy production. The most efficient way to convert hydrogen back to electricity is via fuel cells, which can be defined as a device that generate electrical energy from a chemical [9] or biochemical [10] reaction. Fuel cells are efficient, clean, and noise free energy generators that convert the chemical energy of a fuel and oxidant into electricity. The fuel cell consists of an anode and cathode, where the oxidation of the fuel and reduction of the oxidant take place, respectively. Both electrodes are typically made of a catalyst layer on top of a gas diffuser, and separated by an electrolyte where the ion exchange occurs to complete the reaction.

There are many types of fuel cell based on the fuel employed such as alkaline (AFC) [11], Phosphoric acid (PAFC) [12], molten carbonate (MCFC) [13] and solid oxide (SOFC) [14].

Polymer Electrolyte Membrane Fuel Cell (PEMFC) [15] has gathered much interest due to its low operating temperature between 60 °C to 80 °C and high versatility [16]. Since the range of energy produced in PEMFC goes from 10^{-3} W to 10^6 W, supplying energy to small electrical devices and up to large systems for energy distribution purposes is possible. In addition, PEMFC has experienced an increased usage as an environmentally sustainable energy generator for various application areas such as transportation, portable electrical devices and stationary energy. Besides, this technology permits the interconnection with others renewable energy sources (generating Hybrid Power systems) with the aim of enhance the energy demand [17-19].

PEMFC can be operated with both hydrogen and alcohols as fuels, but hydrogen [20] produces a higher power density than alcohol [21]. It is well known that the determining process in PEMFC is the cathodic process, where the Oxygen Reduction Reaction (ORR) takes place with a lower rate constant than fuel oxidation [22]. The main mechanisms on the electrochemical ORR leads to two main applications: (1) ORR via 4 electrons leading to H_2O and heat generation, this approach is employed in energy conversion, such as in PEMFC [23]; (2) ORR via 2 electrons leading to H_2O_2 generation, this approach is employed in environmental and synthesis applications, since H_2O_2 produced is a powerful oxidant reagent [24, 25].

The operational performance of the cell is influenced by different parameters such as, temperature of the cell, gas feeding and design of the flow plates [16, 26], water management [27], pressure of the gases [28] and activity of the catalyst [29].

The improvement on the catalytic activity for the ORR represents one of the important studies in fuel cell development. Pt based electrocatalysts are the most reported materials for ORR [29] because of their high stability, kinetic activity, etc. Efforts to increase the catalytic activity for ORR include improved catalyst utilization, higher electroactive surface area, homogeneous catalyst distribution, and higher electrical contact between the Pt particles. To achieve these targets, the utilization of improved catalyst supports based on carbon structures such as Multiwalled Carbon Nanotubes (MWCNT) [30], Single wall Carbon Nanotubes (SWCNT)

[31], graphene oxide film [32], Vulcan [33] and Graphite [34] have been reported with different results. MWCNT have shown excellent electrical properties, extraordinary thermal conductivity [35] and good mechanical properties [36] making them a good candidate for catalyst support [37] in fuel cells.

Other areas of research in the catalyst activity improvement are: to decrease the catalyst particle size [38], structural change to increase electrochemical active area, to improve durability due to CO poisoning and increase the active sites [39]. In the catalyst layer, research has been focused on increasing the contact between the support and the catalyst particles to reduce the resistance to charge- and mass-transfer, and to increase gas-diffusion channels, with the main objective of enhancing the ohmic contact in the triple-phase boundary (catalyst, ionomer and support) within the catalyst layer structure [40]. There exist other areas of PEMFC improvement such as, the development of alternatives to Pt to reduce catalyst cost such as, non-noble materials [41], organometallic complexes [42] and alloy materials [43], including alloying with other metals and core-shell nanocatalysts [44, 45]. Fang *et al.* [46] reported the evaluation of the performance in a PEMFC of an assembly fabricated with Pt/C (ETEK) as anode and Pt_{51}-Au_{49}/C (20wt%) as cathode with active area of 5 cm^2; the evaluation was performed at 75 °C, 30 lb in^{-2} H_2/O_2 and 0.40 mg_{Pt} cm^{-2}, obtaining current and power densities values around 1400 mA cm^{-2} at 0.5 V and 640 mW cm^{-2}, respectively. So-Mi *et al.* [47] synthesized a catalyst based on Platinum and gold supported on carbon with various Pt/Au ratios by reduction method, these materials were evaluated as catalysts in the ORR and it reached a maximum when Pt/Au ratio was 90/10. Also, an assembly was made with Pt/C (ETEK) and Pt_{90}-Au_{10}/C (20 wt%) as anode and cathode, respectively, and active area of 5 cm^2 to evaluate in a PEMFC at 70 °C, 400 mL min^{-2} H_2 and 1300 mL min^{-2} O_2, platinum loading of 0.40 mg_{Pt} cm^{-2}. The maximum power density reached was 370.3 mW cm^{-2} and current density value of 800 mA cm^{-2} at 0.5 V.

This work presents the synthesis of composite bimetallic nanoparticles based on platinum and gold supported on MWCNT (Pt-Au/MWCNT) with atomic ratio Pt-Au (1:1) and 20 wt% of metal loading (Pt-Au) with 80 wt% of MWCNT by the reverse microemulsion method to be used as electrocatalysts in the cathode of a single PEMFC. The nanomaterials of Pt-Au/MWCNT and commercial Pt on Vulcan XC-72 carbon (Pt/C) were characterized by physicochemical methods. Electrochemical measurements such as thin-film rotate disk electrode (RDE) and electrochemical active surface area (S_{EI}) were performed in order to compare the catalytic activity for ORR and understand the pathway of the ORR using Koutecky-Levich equation. Furthermore, Membrane Electrode Assemblies (MEAs) prepared using Pt-Au/MWCNT and Pt/C as cathode and anode, respectively and Pt/C as both cathode and anode were compared through electrochemical tests in a single fuel cell hardware. Catalyst ink with various Nafion® concentrations such as 3 wt%, 6 wt%, 16 wt% and 26 wt% was varied in the cathode to study the influence of its concentration on the performance of the MEAs.

2. Materials and methods

2.1 Chemicals

Potassium hexachloroplatinate (IV) ($K_2PtCl_6 \cdot xH_2O$, 98%), Chloroauric Acid ($HAuCl_4 \cdot xH_2O$, 99%) sodium citrate tribasic hydrate ($C_6H_5Na_3O_7 \cdot xH_2O$, 99%), Hexadecyltrimethylammonium bromide (CTAB, 99%), Ferrocene ($C_{10}H_{10}Fe$, 98%) and Nafion® solution (5 wt%) were purchased from Sigma-Aldrich. Sodium borohydride ($NaBH_4$, 98%), sulfuric acid (H_2SO_4, 97%), nitric acid (HNO_3, 70%), isopropanol (C_3H_8O, 99%), methanol (CH_3OH, 99.9%), ethanol (C_2H_5OH, 99%), toluene (C_7H_8, 99.5%) and acetone (C_2H_6O, 99%) were acquired from Fermont. Nitrogen gas (99%), oxygen gas (99%), argon gas (99.9%), hydrogen gas (99%) and liquid nitrogen (99.999%) were supplied by Industrial Gases Infra. All chemicals were used as received. Clear fused quartz tube was purchased from AdValue Technology. Gas diffusion layer (SGL carbon 34BC) with air permeability of 0.35 ± 0.25 cm^3 cm^{-2} s^{-1} was acquired from Ion Power, Inc. Commercial Pt/C was acquired from Fuel Cell Store. Nafion R212 Membrane was supplied by Dupont. Aqueous solutions and water used in synthesis of nanomaterials were prepared with Milli-Q water (18 MΩ, Millipore).

2.2 Synthesis of the nanomaterials

2.2.1 Synthesis, purification and functionalization of MWCNT

MWCNT were synthesized by the spray pyrolysis technique, as reported by Alonso-Núñez *et al* [48]. The solution containing 25 mM of ferrocene in toluene was nebulized and transported to a quartz tube by argon flow at 20 psig, the flow injection was controlled by a rotameter at 6.37 cm^3 h^{-1}. The quartz tube was previously heated at 850 °C in an oven (Thermo Scientific model Lindberg/Blue M) to start the synthesis and the reaction time was fixed to 30 min at the aforementioned conditions. Then, the reactor was allowed to cool in argon atmosphere until it reaches room temperature.

Purification/functionalization of MWCNT support which acts as the support for platinum nanoparticles are required to remove the residues derived from the synthesis and creates

active sites to attach the nanoparticles onto the support. The process was carried as follows: a solution of 3 M HNO_3/1 M H_2SO_4 was mixed with 2 mL of CH_3OH to eliminate residual contents of Fe in 100 mg of MWCNT (Fe is associated with the ferrocene used in the synthesis of MWCNT) by reflux for 120 min. Finally, the purified/functionalized MWCNT was rinsed with water, methanol and acetone by using a filtering system and allowed to dry for 24 h at 100 °C.

2.2.2 Synthesis of Pt-Au/MWCNT nanomaterial

Once MWCNT were synthesized and functionalized, the synthesis of the nanomaterial was carried out. Since commercial Pt/C has a platinum loading of 20 wt%, the aim of the synthesis by reverse microemulsion was to obtain the same loading (20 wt%) of nanosized Pt-Au on the MWCNT with atomic ratio Pt:Au (1:1). Reverse microemulsion proved to be an effective method for good dispersion and synthesis of smaller size nanoparticles [49]. Our group has reported the synthesis of bimetallic electrocatalysts for H_2O_2 generation by reverse microemulsion [24, 25]; however, those reports are referred to 20 mg of the nanomaterial with different synthesis procedures. In this work, the synthesis was scaled up to obtain 100 mg of Pt-Au/MWCNT nanomaterial starting with 80 mg of MWCNT support.

The nanoparticle deposition on MWCNT procedure begins with the preparation of solution A, consisting of CTAB/isopropanol/water in 4.8/88.9/6.3 (v/v%), respectively. 80 mg of MWCNT in 170 mL of solution A were dispersed in ultrasonic bath for 45 min. The dispersed slurry was stirred and refluxed for 10 min in a round bottom flask of 1.0 L with three necks. Simultaneously, two different microemulsion solutions were prepared, a solution of K_2PtCl_6 (9.8 mM) in 40 mL of solution A and the reducing solution, which consisted of $NaBH_4$ (50 mM) and $C_6H_5Na_3O_7$ (50 mM) in 40 mL of solution A. The reducing solution was then added to the slurry, after stirring by 20 min, the K_2PtCl_6 solution was added. Finally, the system was left standing to react for 3 h. After that, a second dose of reducing solution $HAuCl_4$ (6.2 mM) was added in 40 mL of solution A and allowed to react by additional 3 h.

The composite Pt-Au/MWCNT obtained from this process was rinsed with water, isopropanol, methanol and acetone, successively, filtered and dried for 24 h at 100 °C.

2.3 Physicochemical and microscopic characterization

Thermogravimetric analysis (TGA) were performed using TA Instrument-Q500 by using a Pt pan of 100 µL Thermograms were recorded in the temperature range of 30 °C to 850 °C, using a heating rate of 20 °C min^{-1} with an oxygen flow of 60 mL min^{-1}.

Transmission Electron Microscopy (TEM) on a JEOL 2200FS with spherical aberration corrector in probe mode was used to observe the morphology of Pt-Au/MWCNT and elemental composition of the samples was made by X-ray dispersive energy (EDS) attached to this equipment.

SEM micrographs were acquired by using a TESCAN VEGA 3, operated at 20 kV and elemental analysis were carried out with Bruker 125 eV detector coupled to the TESCAN microscope to observe the microstructure of the MEAs.

2.4 MEAs preparation

MEAs were prepared applying the catalyst ink onto the Gas Diffusion Layers (GDL) with metal loading on the GDL of 0.5 mg cm^{-2} to obtain the cathode and anode Gas Diffusion Electrodes (GDE) followed by hot-pressing with the membrane in between, to form a 5-layer MEA with an active area of 9 cm^2. More details of this and other methods to prepare MEAs are described in [50-52]. In all the MEAs prepared, only Pt-Au/MWCNT was used as cathodic electrocatalyst, while the commercial Pt/C was used as anodic electrocatalyst.

The Pt/C catalyst ink was prepared by mixing the Pt/C nanomaterial with a solution of water, Nafion® solution (5 wt%) and ethanol in a 1:4:1.4:20 by weight ratio, respectively. However, the catalytic ink ratio was changed (1:1.4:20:212) for Pt-Au/MWCNT to ensure a homogenous dispersion. The amount of Nafion® solution was varied: 3 wt%, 6 wt%, 16 wt% and 26 wt% to study the influence of its concentration on the performance of the MEAs.

2.5 Electrochemical measurements

All electrochemical measurements were performed in a three-electrode cell, which contained a Pt Rotating Disk Electrode (RDE) as the working electrode (WE, geometric area, 0.1257 cm^2), $Ag/AgCl/KCl_{(saturated)}$ as the reference electrode (RE) and a Pt spiral wire with large surface area as counter electrode (CE). These electrodes were immersed in 0.5 M H_2SO_4 solution at room temperature. The electrochemical system was connected to a potentiostat/galvanostat Biologic model VMP-300. All potential values were referred to the Standard Hydrogen Electrode (SHE).

In order to perform the electrochemical measurements, the Pt RDE surface was first polished with an alumina slurry (0.05 µm grade), and then, the electrode was prepared with 40 µL of a catalytic ink prepared by suspending 2 mg of

either Pt-Au/MWCNT or Pt/C in a solution of 150 µL of Nafion® (5 wt%) and 550 µL of ethanol. The ink was sonicated before the deposition on the electrode to obtain a homogenous ink.

The MEAs fabricated with these two catalysts (commercial Pt/C and Pt-Au/MWCNT), were characterized in a single fuel cell hardware (in-house design), in order to compare their performance and also to correlate these results with the kinetic results obtained in the RDE study. The fuel cell tests were carried out by using a potentiostat/galvanostat Solartron model 1287 with 20A booster attached, Solartron model 1290 and an Impedance/Gain-phase analyzer Solartron model 1260.

2.5.1 S_{EI} and ORR activity

Measurement of Electrochemical active surface area (S_{EI}) is based on the integrated charge in hydrogen underpotential deposition (H-UPD) in platinum. Ye *et al* [53] reported S_{EI}, accordingly to Eq. 1:

$$S_{EI} = Q_H / Q_{ref} * Pt_{load} \quad (1)$$

Where S_{EI} is reported in $m^2\ g^{-1}$, Q_H is the integrated charge in H-UPD region (mC), Q_{ref} is the integrated charge for the adsorption/desorption of one monolayer of hydrogen in Pt (111), which is a constant value of 0.21 mC cm^{-2} and $Pt_{loading}$ is the mass of Pt placed onto working electrode (mg).

To carry out SEI measurements, cyclic voltammetry (CV) in 0.5 M H2SO4 solution were recorded in the potential range of 0.0 V to 1.4 V vs SHE, at scan rate of 100 mV s-1.

For ORR catalytic activity test, 0.5 M H_2SO_4 solution was bubbled with oxygen gas for 20 min. Then, linear sweep voltammetry (LSV) were recorded in a potential range of 1.0 V to 0.1 V vs SHE, at scan rate 5 mV s^{-1}. Also, different rotation speeds of the Pt-modified RDE (50, 100, 250, 500, 750 and 1000 rpm) were applied in order to analyze the results by Koutecky-Levich equation [54].

2.5.2 Fuel cell testing protocol

The ohmic resistance was measured with an Electrochemical Impedance Spectroscopy (EIS) in the frequency range of 100 kHz to 0.1 Hz with 10 mV ac, at 0 V dc and 10 steps dec^{-1}. The fuel cell hardware is fed with oxygen (cathode) and hydrogen (anode), both at 10 psig and heated at 60 °C.

The MEAs performance was measured by potentiodynamic polarizations from OCV to 0.1 V, with a scan rate of 2 mV s^{-1} to obtain the polarization (I-V) curve by triplicate for each sample, at 60 °C and 10 psig for H_2 and O_2.

The active surface area (ESA) is an analog test to determine the electrochemical active surface area (S_{EI}) performed in the fuel cell hardware. In ESA, cyclic voltammetry is recorded, supplying nitrogen gas at cathode and hydrogen at anode, the charge integrated in the potential range from 0.0 to 0.3 V is related to H_2 adsorption/desorption in the anode.

3. Results and Discussion

3.1 TGA analysis

In order to confirm the amount of metallic content (Pt and Pt-Au) and the thermal behavior of the MWCNT and the C Vulcan, TGA analysis was performed. It is important to point that this technique is non-selective to each metallic species for Pt-Au/MWCNT. Fig. 1 shows the thermograms for Pt-Au/MWCNT and Pt/C. The thermogram corresponding to Pt/C shows a weight loss at 400 °C is attributed to the combustion of the Vulcan carbon [55]. The remaining weight of 19.35% is associated with the corresponding metallic oxide (PtO_2) while the thermogram corresponding to Pt-Au/MWCNT shows a weight loss at 580 °C associated with MWCNT combustion [55]. The final of 25.00% weight loss is attributed to the corresponding metallic oxides (PtO_2 and Au_2O_3). However, it is not feasible to accurately determine the individual concentration for each element.

3.2 STEM microscopy

The morphology and the size distribution of the nanoparticles anchored on the MWCNT were determined by STEM mode images. The micrographs of the Pt-Au/MWCNT electrocatalyst clearly shows the uniformly dispersion of Pt-Au on the MWCNT creating a multi-dimensional network structure that facilitates the electrons/

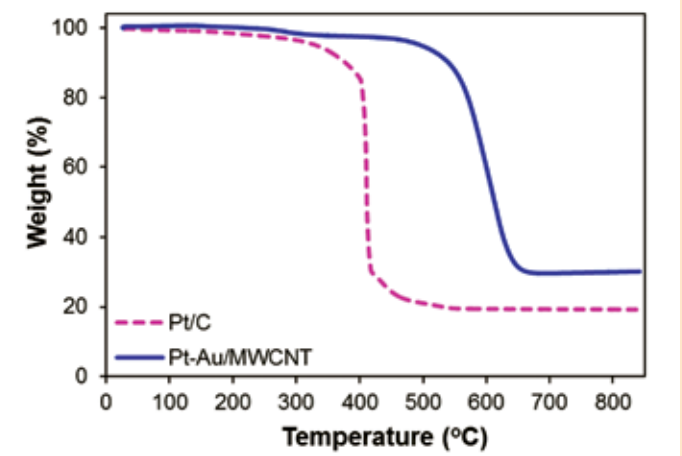

Fig. 1. TGA curves for PteAu/MWCNT and Pt/C nanomaterials.

protons transfer and increasing the active sites (Fig. 2a and 2b). The porosity of catalyst/MWCNT network in combination with the placement of catalyst particles closer to nanotubes edges provides effective triple phase formation and transfer of gas and water, thereby, reducing the ohmic resistance and promoting electronic and ionic transfer. The TEM images confirmed a good distribution of the bimetallic particles. Fig. 2c shows the particle size Gaussian distribution with an average diameter of 3.26±0.47 nm for Pt-Au nanoparticles. The Fig. 2d and Fig. 2e shows the lower and higher magnification of Pt/C commercial nanoparticles on Vulcan carbon with a good deposition of Pt on the carbon support. At low magnification, uniform dispersion is observed and at high magnification the particles do not overlay. However, large aggregation of Pt particles makes it difficult for the reactants to access the active sites and causing reduced catalyst utilization. Fig. 2f shows the particle size distribution for Pt with average diameter of 1.76±0.33 nm.

The composition analysis was performed by EDS and Fig. 3 shows the typical elemental composition spectrum of Pt-Au/MWCNT. The average elemental composition was obtained from 12 different zones analyzed in the sample. The EDS spectra for Pt-Au/MWCNT showed 54.13% of Pt and 45.87% of Au In close agreement with the original Pt:Au ratio (1:1) of the precursor synthesis solution.

According to STEM micrographs and EDS elemental analysis, it can be seen that the Pt commercial particle size is smaller than Pt-Au alloy. However, Pt-Au particles on MWCNT have better performance in the fuel cell hardware. Matsumoto *et al.* [56], Zhao *et al.* [57] and Wu *et al.* [42] have also shown better performance when carbon nanotubes are used as the support material.

3.3 Electrocatalytic activity for ORR

3.3.1 Electrochemically active surface area of the electrocatalyst

Fig. 4 shows cyclic voltammograms for Pt-Au/MWCNT and Pt/C. Both electrocatalysts show hydrogen adsorption/desorption features in the potential range of 0.0 V to 0.3 V vs SHE. The reduction peak potential of Pt_xO_y is located at 0.65 V vs SHE in both electrocatalysts. Herein, the S_{EI} values for both electrocatalysts are calculated according to Eq. 1, where, Q_H for Pt-Au/MWCNT and Pt/C (commercial) were 7.33 mC and 8.69 mC, respectively. From TGA analysis and elemental average value from EDS, the $Pt_{loading}$ of Pt-Au/MWCNT and Pt/C (commercial) were estimated to be 0.02 mg for both electrocatalysts. The S_{EI} values estimated were found 24.93 $m^2\ g^{-1}$ for Pt-Au/MWCNT and 27.39 $m^2\ g^{-1}$ for Pt/C (commercial).

3.3.2 Oxygen Reduction Reaction for the electrocatalyst

In order to measure the catalytic activity in the ORR for the electrocatalysts, LSV were performed using the RDE technique. Fig. 5a and 5b shows the voltammograms for Pt-Au/MWCNT and Pt/C, respectively. It is noticeable that the onset potential for ORR was around 0.8 V vs SHE for both samples. Also, the electrocatalysts showed no significant

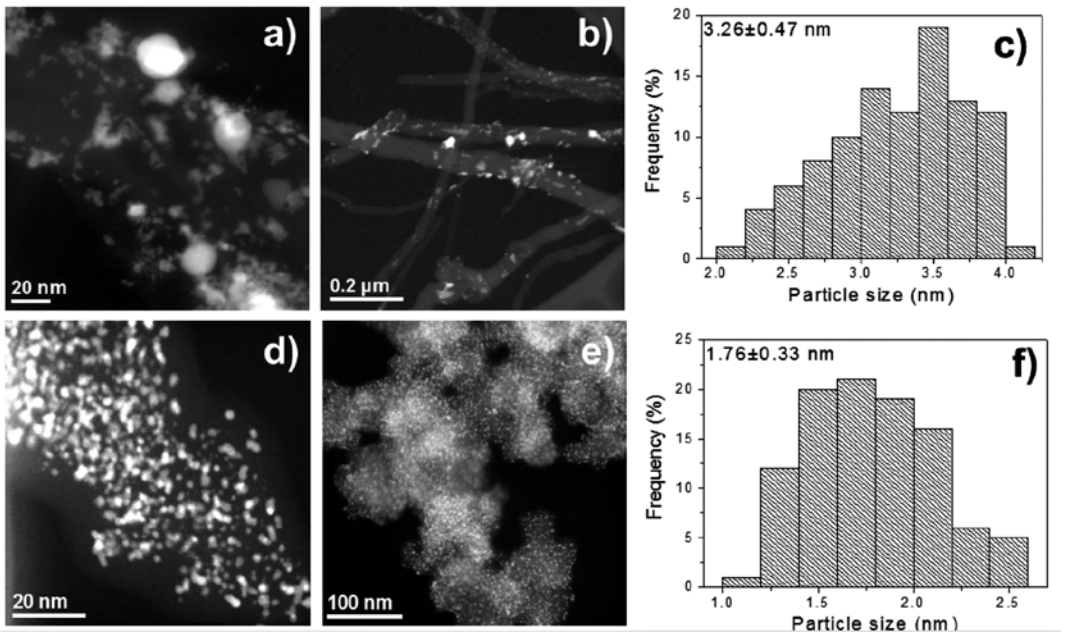

Fig. 2. TEM images of (a and b) PteAu/MWCNT and (d and e) Pt/C commercial; Histogram of the size distribution of (c) PteAu/MWCNT nanomaterial and (f) Pt/C commercial.

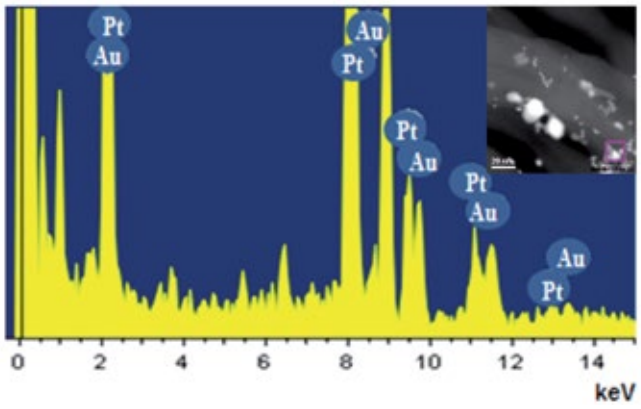

Fig. 3. EDS and HAADF image of one zone of PteAu/MWCNT nanomaterial.

difference in the diffusion limiting current density at 1000 rpm (or plateau current density).

The kinetic current density [54] at 0.7 V can be defined as (Eq. 2):

$$j_{k,0.7V} = j_D * j_{0.7V} / j_D - j_{0.7V} \quad (2)$$

Where $j_{k,0.7V}$ is the kinetic current density at 0.7 V (mA cm^{-2}), j_D is the diffusion limiting current density (mA cm^{-2}) and $j_{0.7V}$ is the current density at 0.7 V. According to Eq. 2, the values of kinetic current density at 1000 rpm were: -7.65 mA cm^{-2} and -3.68 mA cm^{-2} for Pt-Au/MWCNT and Pt/C (commercial), respectively. Lin *et al.* [58] reported nano-structured catalysts based on carbon-supported Au@Pt core shell with varying the atomic ratio of Pt:Au synthesized by the seed-mediated growth method; the best catalytic activity for ORR obtained was for Au@Pt(2:4)/C catalyst, the current density value exhibited was around -4 mA cm^{-2} at 0.1 V vs SHE and 1800 rpm.

ORR is a complex process that involves different pathways [59]. In order to clarify the mechanism of ORR, Koutecky-Levich equation was used to determinate the number of electrons transferred (n) during the ORR; this equation states an inverse ratio between the reciprocal of the current density and the square root of the rotation speed (Eq. 3):

$$1/J = 1/J_k + 1/B\,\omega^{1/2} \quad (3)$$

Where J (mA cm^{-2}) is the experimentally observed current density, J_k is the kinetic current density (mA cm^{-2}) and ω is the rotation speed of the RDE (rpm). When this relationship is plotted, n in the ORR can be calculated from the slope, according to Eq. 4:

$$B = 0.20nFD^{2/3}_{O2}\upsilon^{-1/6}CO_2 \quad (4)$$

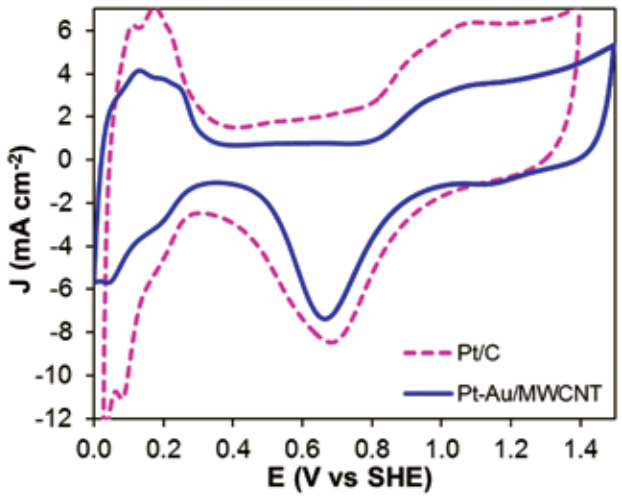

Fig. 4. Cyclic voltammograms of PteAu/MWCNT and Pt/C (commercial) electrocatalysts in 0.5 M H_2SO_4 at scan rate of 100 mV s^{-1}.

The coefficient *0.20* is used when ω units are rpm, n is the number of electrons transferred, D_{O2} is the diffusion coefficient for oxygen (1.85 x 10^{-5} cm^2 s^{-1}), υ is the kinematic viscosity of H_2SO_4 solution (0.01 cm^2 s^{-1}) and C_{O2} is the concentration of dissolved oxygen in the solution (1.13 x 10^{-6} mol cm^{-3}). Fig. 5c shows the Koutecky-Levich plots for Pt-Au/MWCNT and Pt/C, where the number of electrons transferred in ORR is close to 4 in both electrocatalysts, leading to H_2O generation. Also Fig. 5d shows that the ORR with 4 electrons transferred occurs in the Pt-Au/MWCNT in a wide potential range (0.1-0.6 V vs SHE), which is recommendable on electrocatalysts for fuel cell application.

Table 1 shows the Koutecky-Levich slope, the experimental number of electrons transferred (n_{exp}) in ORR, and the kinetic rate constant (k) values derived from the intercept term in Koutecky-Levich equation for Pt-Au/MWCNT and Pt/C. It is noticeable that a higher value of the kinetic rate constant is observed for Pt-Au/MWCNT than for Pt/C (commercial), which could be due to a synergistic effect of the bimetallic alloying character.

3.4 Fuel cell test

3.4.1 Comparison of Pt-Au/MWCNT and Pt/C

The performance of the Pt-Au/MWCNT as cathode catalyst in a single fuel cell was compared with the Pt/C commercial, Fig. 6a shows the peaks attributed to hydrogen adsorption/desorption between 0.0 to 0.3 V. The charge integrated for hydrogen desorption is related to Electrochemical Surface Area (ESA) values. ESA values found were similar for both electrocatalysts, 0.45 mC cm^{-2} for Pt-Au/MWCNT and

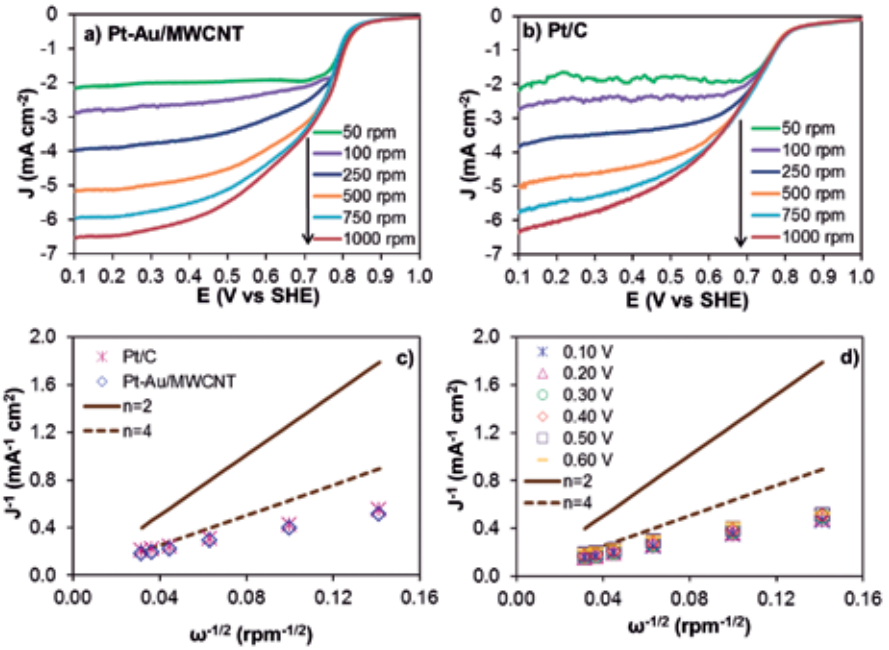

Fig. 5. Linear voltammograms recorded in O_2 saturated H_2SO_4 (0.5 M) at different rotation speeds for (a) Pt–Au/MWCNT, (b) Pt/C at scan rate of 5 mV s^{-1}, (c) Koutecky-Levich plot for Pt–Au/MWCNT (◊) and Pt/C (*) determined at 0.5 V vs SHE and (d) Koutecky-Levich plot for Pt–Au/MWCNT at different potentials.

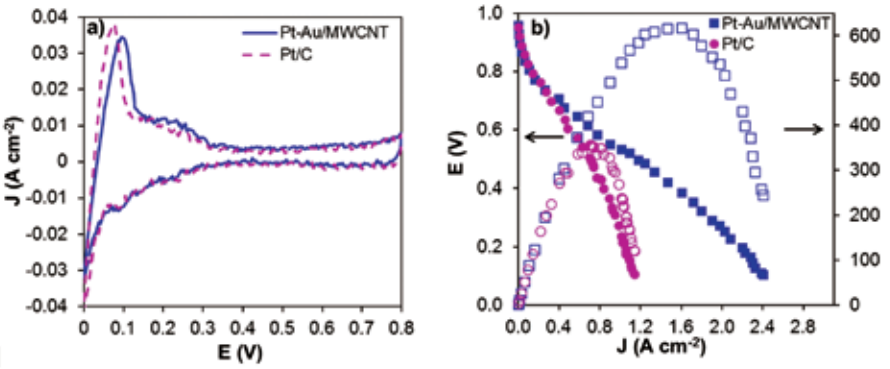

Fig. 6. (a) Adsorption/desorption region of Pt–Au/MWCNT and Pt/C; (b) Polarization curves (filled) and power densities (blank) for both assemblies.

0.43 mC cm^{-2} for Pt/C (commercial). However, Fig. 6b demonstrates that better fuel cell performance is obtained by using Pt-Au/MWCNT as cathode than Pt/C (commercial) since the maximum power density values were 625 mW cm^{-2} at 0.426 V for Pt-Au/MWCNT and 355 mW cm^{-2} at 0.499 V for Pt/C (commercial) (Table 2). These values were obtained from the polarization curve (Fig. 6b), where the ohmic and mass transport overpotentials are higher for Pt/C (commercial) than Pt-Au/MWCNT cathode. Assuming that both MEAs had the same humidity content during the test (pre conditioning process as part of testing protocol) and similar triple-phase boundary areas, the better performance of Pt-Au/MWCNT could be due to good ohmic contact along the catalyst layer facilitated by the location of the catalyst particles along the edges of the MWCNT and a better 3-D structure. Furthermore, in the mass transport overpotential zone, it could be hypothesized that a thinner thickness of the Pt-Au/MWCNT catalyst layer (Table 3) not only benefited the utilization of the catalyst sites but also reduced the path to the reactant gases to the reaction sites. The higher porosity in the structure of the Pt-Au/MWCNT catalyst layer (compare Fig. 7c and 7e) produced a lower mass transport resistance than the Pt/C catalyst layer, as observed at moderate currents in Fig. 6b, where the voltage dropped faster for Pt/C than for Pt-Au/MWCNT due to the mass transport limitations. It also can be inferred form the low currents region in Fig. 6b that the curves slopes for both catalyst layers (Pt/C commercial and Pt-Au/MWCNT) were similar, although, pointing to similar activation overpotentials in fuel cell. Lin *et al.* [58] performed the evaluation of Au@Pt (2:4)/C as catalyst in a PEMFC reaching a maximum power density value of 479 mW cm^{-2} using H_2 and O_2 at 80 °C. Also, Selvarani *et al.* reported a catalyst based on Pt-Au (3:1) supported on carbon (Pt-Au/C), which was used as cathode in PEMFC, the maximum power density obtained with this catalyst was 650 mW cm^{-2} using H_2 and O_2 at 60 °C, the amount of the platinum is higher than catalyst reported in this work [60].

3.4.2 Variation of Nafion® solution content in the catalytic ink

Fig. 8a shows the signals attributed to hydrogen adsorption/desorption between 0.0 to 0.3 V of some fabricated MEAs with different concentration of Nafion® solution in the catalytic ink (the other components: Pt-Au/MWCNT, ethanol, and water were maintained

Table 1
Experimental parameters for PteAu/MWCNT and Pt/C (commercial) determined from Koutecky-Levich plot.

Sample	Experimental slope	n_{exp}	k (cm s^{-1})
Pt/C (Commercial)	3.15	5.00	1.73 X 10^{-2}
Pt-Au/MWCNT	3.20	4.98	2.26 X 10^{-2}

Table 2
Different performance parameters for PteAu/MWCNT and Pt/C (commercial) with 6 wt% of Nafion® in the fuel cell test.

Assembly	OCP (V)	R (Ω)	J (A cm^{-2}, E = 0.5V)	J (A cm^{-2}, E = 0.1 V)	P (mW cm^{-2})
Pt/C (commercial)	- 0.97	0.24	0.71	1.07	355
PteAu/ MWCNT	- 0.96	0.20	1.14	2.34	625

Table 3
Effect of Nafion® content on catalytic layer thickness and different performance parameters in fuel cell test for PteAu/MWCNT with different wt% of Nafion® solution.

Nafion® content (wt%)	Estimated catalytic layer thickness (mm)		OCP (V)	R (Ω)	J (A cm^{-2}, E = 0.5 V)	J (A cm^{-2}, E = 0.1 V)	P (mW cm^{-2})
	Pt/C (anode)	Pt–Au/ MWCNT (cathode)					
3	25	22	- 0.95	0.22	0.77	1.82	424
6	24	15	- 0.96	0.20	1.14	2.34	625
16	16	11	- 0.96	0.24	0.71	1.70	396
26	17	11	- 0.96	0.21	0.65	1.73	364

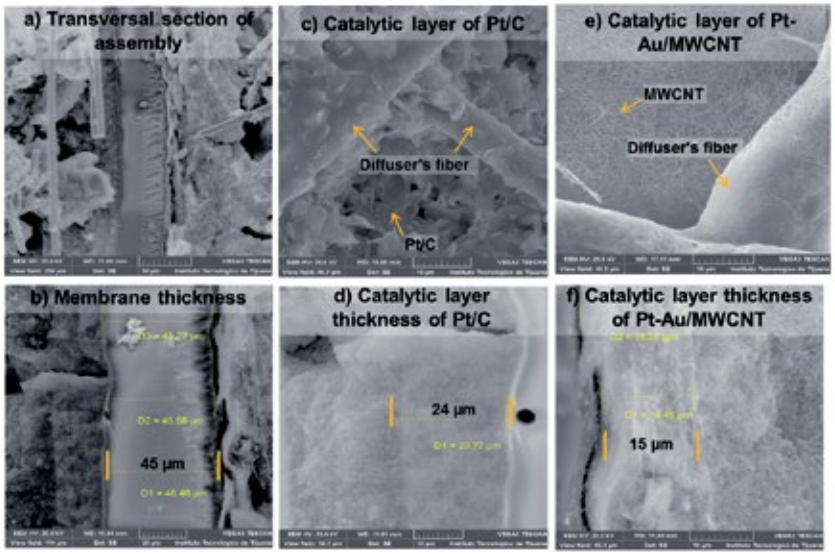

Fig. 7. SEM images of the assembly with Pt–Au/MWCNT (cathode) and Pt/C (anode).

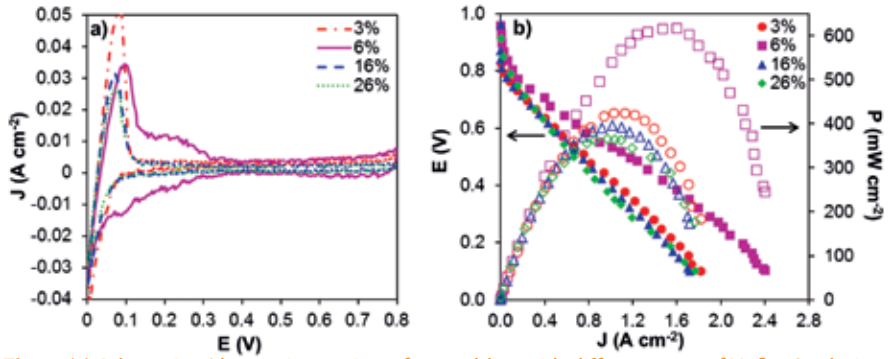

Fig. 8. (a) Adsorption/desorption region of assemblies with different wt% of Nafion® solution and (b) Polarization curves (filled) and power densities (blank) of the assemblies.

constant as defined in section 2.5). It is well known that the composition of catalytic ink solution is an important challenge to improve fuel cells manufacturing and an attempt was made in this paper to understand their influence in the performance of the cathode. The concentrations of Nafion® solution used here were: 3, 6, 16, and 26 wt% and their corresponding ESA values were: 0.37 mC cm^{-2}, 0.45 mC cm^{-2}, 0.25 mC cm^{-2} and 0.21 mC cm^{-2}, respectively. It is clearly evident that the MEA with 6 wt% of Nafion®, had the widest region associated with the adsorption and desorption of hydrogen and obtained the highest ESA value (see Fig. 8a). Likewise, the Fig. 8b shows the polarization (I-V) and power density curves for the MEAs with variation of Nafion® solution. Similarly, the MEA with 6 wt% of Nafion® showed the best performance in the I-V curve, with 1.14 A cm^{-2} at 0.5 V and the highest maximum power density with 625 mW cm^{-2}, is noticeable that this catalyst reach practically the same maximum power density value than the reported by Fang et al., however that value is obtained at 75 °C, while the value reported in this work was obtained at 60°C [46]. Table 3 shows the performance parameters of all MEAs with different concentrations of Nafion® solution. These results confirmed the impact on the PEMFC performance by the concentration of Nafion® solution in the catalyst layer.

It is also very well known that the amount of Nafion® affects the mass transport and the ionic conductivity in the triple phase boundary areas within the catalyst layer and across the membrane interface [61]. Several studies suggest that there is an optimal amount of Nafion® up to a critical ratio at which the Nafion® (ionomer) begins to create a mass transport barrier and higher electronic impedance [62-65]. An insufficient amount of Nafion®

results in a poor triple phase boundary presence, limiting the platinum activity even though there is an even particle distribution. This phenomenon could explain the lower ESA obtained for the MEA with 3 wt% of Nafion® compared to the MEA with 6 wt% of Nafion® (see Fig. 8a). On the other hand, excess Nafion® blocks the pores of the catalyst layer, masks the catalyst particles, hinders the path of the reactant gas to the active sites, and also increasing the water content in the catalyst layer. These are the impacting factors for the MEA performance and the hydrogen adsorption/desorption (see Fig. 8a). Likewise, the lower performance obtained in the MEAs with Nafion® concentrations of 3, 16 and 26 wt% in the I-V curve confirm that Nafion® plays an important role for both the ohmic and mass transport regions showing a similar voltage drop (similar slope) after the active polarization region, with the best performance for MEA with 6 wt% of Nafion® (see Fig. 8b).

3.4.3 SEM micrographics of MEAs

SEM and EDS analysis were performed in order to measure the thickness of the catalytic layer in both diffusers of MEA. The thickness of the catalytic layer was estimated by determining the presence of Pt and Pt-Au at different distances from the surface until Pt and Pt-Au were no longer detected. This profile of catalytic layer (distance wise) from the surface of the GDL is related to the ink solution application method; the porosity of the GDL, the catalyst material (Pt/C or Pt-Au/MWCNT) and the composition of the ink solution (Nafion® content). Fig. 7 shows micrographs for a MEA (Nafion® 6 wt%), where the thickness of the Nafion membrane was 45.8 μm, the thickness of the catalytic layer had a thickness of 23.8 μm for Pt/C (commercial), while for Pt-Au/MWCNT was found in 15.4 μm. Table 3 shows values of different parameters of MEAs prepared by varying the content of Nafion® in catalytic ink. When Nafion® content was increased, the thickness of the catalytic layer decreased and the power density of the cell varied, reaching a maximum value when a 6 wt% of Nafion® content was used. These results could be linked to the porosity of the catalyst layer, as the MWCNT has a more compact system compared to the Vulcan carbon, demonstrated a thinner layer with better repercussions in the ohmic contact.

4. Conclusions

Although there are few reports with Pt-Au catalyst in literature, no reports of this material is reported by using MWCNT as support. The synthesis of Pt-Au/MWCNT by using reverse microemulsion methodology and their performance was compared with Pt/C (commercial). The experimental characterization indicates a good dispersion, size distribution and adequate total amount of metal content of the nanomaterial. Moreover, the elemental average value from EDS confirms that the composition of Pt:Au is approximately 1:1.

Electrochemical measurements were performed in order to compare the catalytic activity in the ORR for Pt-Au/MWCNT and Pt/C (commercial). No significant differences were observed in S_{EI}, onset potential and diffusion limiting current density in both electrocatalysts. However, the value of kinetic density current at 0.7 V is higher in Pt-Au/MWCNT than Pt/C (commercial), this fact is attributed to an improvement in the electronic charge transference by using MWCNT as support, compared with other carbonaceous materials. ORR with 4 electrons transferred took place in both electrocatalysts leading to H_2O. Furthermore, ORR process with 4 electrons occurred in a wide range of potential in Pt-Au/MWCNT, which means this electrocatalyst is a promising alternative to Pt/C for fuel cell application.

A critical parameter in the catalyst performance is the adequate quantity of Nafion, in this paper were studied different Nafion® concentration, the MEA with 6 wt% of Nafion® showed the best performance in a single fuel cell hardware working with H_2 and O_2. Even with the same value of ESA, Pt-Au/MWCNT exhibited a better performance in single fuel cell test. An explanation based on the thinner catalyst layer obtained with the alternative Pt-Au/MWCNT and its multi-dimensional network is believed to have facilitated transportation of gases and water, ensuring reactants to reach the catalyst sites.

Acknowledgements

We would like to take this opportunity to thank Consejo Nacional de Ciencia y Tecnología (CONACyT) under grants projects INFR-2014-224627 and RED-2012-194153 and Tecnológico Nacional de México (TNM) under grant TNM-5626.15-P for supporting this research project. Mara Beltrán-Gastélum is grateful to CONACyT for providing the scholarship for her doctoral thesis research. Thanks to Nanotechnology National Lab, located at CIMAV, Chihuahua, México, for electron microscopy study, thanks for their technical help to W. Antunez, E. Lestarjette, P. Pisa and C. Ornelas. The authors thank to S. Velraj for comments and review of the manuscript.

References

[1] Meier JC, Galeano C, Katsounaros I, Topalov AA, Kostka A, Schüth F, Mayrhofer KJJ. Degradation Mechanisms of Pt/C Fuel Cell Catalysts under Simulated Start–Stop Conditions. Catal. 2012;2:832-43.

[2] Pethaiah SS, Gangadharan S, Hwa Chan S, Stimming U. Development of a novel cost effective methanol electrolyzer stack with Pt-catalyzed membrane. J. Power Sources 2014;254:161-7.

[3] Dell RM, Bridger NJ. Hydrogen- the ultimate fuel. Appl. Energy 1975;1(4):279-92.

[4] Yuzbasi NS, Selçuk N. Air and oxygen-fuel combustion behavior of petcoke/lignite blends. Fuel 2012;92:137-44.

[5] Geisler C, Hördt W, Kluska S, Mondon A, Hopman S, Glatthaar M. Overcoming electrical and mechanical challenges of continuous wave laser processing for Ni-Cu plated solar cells. Sol. Energy Mater. Sol. Cells 2015;133:48-55.

[6] Jolly S, Raven RPJM. Collective institutional entrepreneurship and contestations in wind energy in India. Renew. Sustainable Energy Rev. 2015:42:999-1011.

[7] Zheng B, Xu J, Ni T, Li M. Geothermal energy utilization trends from a technological paradigm perspective. Renew. Energy 2015;77:430-41.

[8] Glotić A, Glotić A, Kitak P, Pihler J, Tičar I. Optimization of hydro energy storage plants by using differential evolution algorithm. Energy 2014;77:97-107.

[9] Fukuyama Y, Shiomi T, Kotaka T, Tabuchi Y. The Impact of Platinum Reduction on Oxygen Transport in Proton Exchange Membrane Fuel Cells. Electrochim. Acta 2014;117:367-78.

[10] Abrevaya XC, Sacco NJ, Bonetto MC, Hilding-Ohlsson A, Cortó E. Analytical applications of microbial fuel cells. Part I: Biochemical oxygen demand. Biosens. Bioelectron. 2015;63:580-90.

[11] Ramanavicius A, Kausaite-Minkstimiene A, Morkvenaite-Vilkonciene I, Genys P, Mikhailova R, Semashko T, Voronovic J, Ramanaviciene A. Biofuel cell based on glucose oxidase from Penicillium funiculosum 46.1 and horseradish peroxidase. Chem. Eng. J. 2015;264:165-73.

[12] Jiao K, Huo S, Zu M, Jiao D, Chen J, Du Q. An analytical model for hydrogen alkaline anion exchange membrane fuel cell. Int. J. Hydrogen Energy 2015;40(8):3300-12.

[13] Zhang H, Lin G, Chen J. Multi-objective optimization analysis and load matching of a phosphoric acid fuel cell system. Int. J. Hydrogen Energy 2012;37(4):3438-46.

[14] Milewski J, Wolowicz M, Miller A, Bernat R. A reduced order model of Molten Carbonate Fuel Cell: A proposal. Int. J. Hydrogen Energy 2013;38(26):11565-75.

[15] Papurello D, Schuhfried E, Lanzini A, Romano A, Cappellin L, Märk TD, Silvestri, S, Santarelli M, Biasioli F. Proton transfer reaction-mass spectrometry as a rapid inline tool for filter efficiency of activated charcoal in support of the development of Solid Oxide Fuel Cells fueled with biogas. Fuel Proc. Technol. 2015;130:78-86.

[16] Carton J, Olabi A. Design of experiment study of the parameters that affect performance of three flow plates configurations of a proton exchange membrane fuel cell. Energy 2010;35:2796-806.

[17] Bruni G, Cordiner S, Mulone V. Domestic distributed power generation: Effect of sizing and energy management strategy on the environmental efficiency of a photovoltaic-battery-fuel cell system. Energy 2014;77:133-43.

[18] Carton J, Olabi A. Wind/hydrogen hybrid systems: Opportunity for Ireland's wind resource to provide consistent sustainable energy supply. Energy 2010;35:4536-44.

[19] Bruni G, Cordiner S, Mulone V, Sinsi V, Spagnolo F. Energy management in a domestic microgrid by means of model predictive controllers. Energy 2015; in press.

[20] Sahoo M, Scott K, Ramaprabhu S. Platinum decorated on partially exfoliated multiwalled carbon nanotubes as high performance cathode catalyst for PEMFC. Int. J. Hydrogen Energy 2015;40:9435-43.

[21] Li W, Xin Q, Yan Y. Nanostructured Pt–Fe/C cathode catalysts for direct methanol fuel cell: The effect of catalyst composition. Int. J. Hydrogen Energy 2010;35:2530-8.

[22] Ahmed MS, Kim D, Jeon S. Covalently grafted platinum nanoparticles to multi walled carbon nanotubes for enhanced electrocatalytic oxygen reduction. Electrochim. Acta 2013;92:168-75.

[23] Oezaslan M, Hasche F, Strasser P. Pt-Based Core–Shell Catalyst Architectures for Oxygen Fuel Cell Electrodes. J. Phys. Chem. Lett. 2013;4:3273–91.

[24] Félix-Navarro RM, Beltrán-Gastélum M, Salazar-Gastélum MI, Silva C, Reynoso E, Pérez-Sicairos S, Lin SW, Paraguay-Delgado F, Alonso-Núñez G. Pt-Pd bimetallic nanoparticles on MWCNTs: catalyst for hydrogen peroxide electrosynthesis. J. Nanopart. Res. 2013;15:1802-12.

[25] Félix-Navarro RM, Salazar-Gastélum MI, Beltrán-Gastélum M, Reynoso E, Lin SW, Pérez-Sicairos S, Paraguay-Delgado F, Alonso-Núñez G. Development of a Pt-Ir Bimetallic Nanoparticulated Electrocatalyst Deposited on MWCNT for an Electro-Fenton Process. J. Electrochem. Soc. 2014;161(12):H845-53.

[26] Carton J, Olabi A. Three-dimensional proton exchange membrane fuel cell model: Comparison of double channel and open pore cellular foam flow plates. Energy 2016;in press.

[27] Carton J, Lawlor V, Olabi A, Hochenauer C, Zauner G. Water droplet accumulation and motion in PEM (Proton Exchange Membrane) fuel cell mini-channels. Energy 2012;39:63-73.

[28] Taymaz I, Benli M. Numerical study of assembly pressure effect on the performance of proton exchange membrane fuel cell. Energy 2010;35:2134-40.

[29] John ST, Angelopoulos AP. In situ analysis of optimum surface atom coordination for Pt nanoparticle oxygen reduction electrocatalysts. Electrochim. Acta 2013;112:258-68.

[30] Kim J, Lee SW, Carlton C, Shao-Horn Y. Pt-Covered Multiwall Carbon Nanotubes for Oxygen Reduction in Fuel Cell Applications. J. Phys. Chem. Lett. 2011;2:1332-6.

[31] Huang M, Dong G, Wu C, Guan L. Preparation of highly dispersed Pt nanoparticles supported on single-walled carbon nanotubes by a microwave-assisted polyol method and their remarkably catalytic activity. Int. J. Hydrogen Energy 2014;39:4266-73.

[32] Gupta VK, Yola ML, Atar N, Üstündağ Z, Solak AO. Electrochemical studies on graphene oxide-supported metallic and bimetallic nanoparticles for fuel cell applications. J. Mol. Liq. 2014;191:172-6.

[33] Weon-Doo L, Dong-Ha L, Hee-Joon C, Ho-In L. Preparation of Pt nanoparticles on carbon support using modified polyol reduction for low-temperature fuel cells. Int. J. Hidrogen Energy 2012;37:12629-38.

[34] Chen M, Lou B, Ni Z, Xu B. PtCo nanoparticles supported on expanded graphite as electrocatalyst for direct methanol fuel cell. Electrochim. Acta 2015;165:105-9.

[35] Datsyuk V, Kalyva M, Papagelis K, Parthenios J, Tasis D, Siokou A, Kallitsis I, Galiotis C. Chemical oxidation of multiwalled carbon nanotubes Carbon 2008;46:833-40.

[36] Ling X, Wei Y, Zou L, Xu S. The effect of different order of purification treatments on the purity of multiwalled carbon nanotubes. Appl. Surf. Sci. 2013;276:159-66.

[37] Hernández-Fernández P, Montiel M, Ocón P, Gómez de la Fuente JL, García-Rodríguez S, Rojas S, Fierro JLG. Functionalization of multi-walled carbon nanotubes and application as supports for electrocatalysts in proton-exchange membrane fuel cell. Appl. Catal. B: Environ. 2010;99:343-52.

[38] Meryemoglu B, Irmak S, Hasanoglu A, Erbatur O, Kay B. Influence of particle size of support on reforming activity and selectivity of activated carbon supported platinum catalyst in APR. Fuel 2014;134:354-7.

[39] Hyuna K, Hee Lee J, Won Yoon C, Cho YH, Kim LH, Kwon Y. Improvement in oxygen reduction activity of polypyrrole-coated PtNi alloy catalyst prepared for proton exchange membrane fuel cells. Synth. Met. 2014;190:48-55.

[40] Zhang J, Tang S, Liao L, Yu W, Li J, Seland F, Haarberg GM. Improved catalytic activity of mixed platinum catalysts supported on various carbon nanomaterials. J. Power Sources 2014;267:706-13.

[41] Wu G, More, KL, Johnston CM, Zelenay P. High-performance electrocatalysts for oxygen reduction derived from polyaniline, iron and cobalt. Science 2011;332(6028):443-7.

[42] Wu X, Xu H, Lu L, Fu J, Zhao H. The study on dynamic response performance of PEMFC with $RuO_2 \bullet xH_2O$/CNTs and Pt/C composite electrode. Int. J. Hydrogen Energy 2010;35:2127-2133.

[43] Shim JH, Kim J, Lee C, Lee Y. Porous Pd layer-coated Au nanoparticles supported on carbon: synthesis and electrocatalytic activity for oxygen reduction in acid media. Chem. Mater. 2011;23(21):4694-700.

[44] Lin R, Zhao T, Shang M, Wang J, Tang W, Guterman VE, Ma J. Effect of heat treatment on the activity and stability of PtCo/C catalyst and application of in-situ X-ray absorption near edge structure for proton exchange membrane fuel cell. J. Power Sources 2015;293:274-82.

[45] Suda Y, Shimizu Y, Ozaki M, Tanoue H, Takikawa H, Ue H, Shimizu K, Umeda Y. Electrochemical properties of fuel cell catalysts loaded on carbon nanomaterials with different geometries. Mater. Today Comm. 2015;3:96-103.

[46] Fang B, Wanjala BN, Hu X, Last J, Loukrapam R, Yin J, Luo J, Zhong CJ. Proton exchange membrane fuel cells with nanoengineered AuPt catalysts at the cathode. J. Power Sources 2011;196:659-65.

[47] So-Mi J, Min-Kyoung K, Gil-Pyo K, Tae-Yun K, Sung-Hyeon B. Preparation of Pt–Au/carbon catalysts by a reduction method and their electrocatalytic activities for oxygen reduction reactions. Chem. Eng. J. 2012;198-199:435-9.

[48] Alonso-Núñez G, Lara-Romero J, Paraguay-Delgado F, Sánchez-Castañeda FM, Jiménez-Sandoval S. Temperature optimization of CNT synthesis by spray pirolisis of alpha-pinene as the carbon source. J. Exp. Nanosci. 2010;5:52-60.

[49] Muralidharan G, Subramanian L, Nallamuthu SK, Santhanam V, Kumar S. Effect of Reagent Addition Rate and Temperature on Synthesis of Gold Nanoparticles in Microemulsion Route. Ind. Eng. Chem. Res. 2011;50:8786-91.

[50] Chaparro AM, Benitez R, Gubler L, Scherer GG, Daza L. Study of membrane electrode assemblies for PEMFC, with cathodes prepared by the electrospray method. J. Power Sources 2007;169(1):77-84.

[51] Taylor AD, Kim EY, Humes VP, Kizuka J, Thompson LT. Inkjet printing of carbon supported platinum 3-D catalyst layers for use in fuel cells. J. Power Sources 2007;171(1):101-6.

[52] Morikawa H, Tsuihiji N, Mitsui T, Kanamura K. Preparation of membrane electrode assembly for fuel cell by using electrophoretic deposition process. J. Electrochem. Soc. 2004;151(10):A1733-7.

[53] Ye W, Kou H, Liu Q, Yan J, Zhou F, Wang C. Electrochemical deposition of Au-Pt alloy particles with cauliflower-like microstructure for electrocatalytic methanol oxidation. Int. J. Hydrogen Energy 2012;37:4088-97.

[54] Xing W, Yin G, Zhang J. Rotating Electrode Methods and Oxygen Reduction Electrocatalyst. 1st ed. Poland: Elsevier B. V.; 2014.

[55] Andersen SM, Borghei M, Lund P, Yli-Rantala E, Pasanen A, Kauppinen E, Ruiz V, Kauranen P, Skou EM. Durability of carbon nanofiber (CNF) & carbon nanotube (CNT) as catalyst support for Proton Exchange Membrane Fuel Cells. Solid State Ionics 2013;231:94-101.

[56] Matsumoto T, Komatsu T, Arai K, Nagashima Y, Yoo E, Yamazaki T, Kijima M, Shimizu H, Takasawa Y, Nakamura J. Efficient usage of highly dispersed Pt on carbon nanotubes for electrode catalysts of polymer electrolyte fuel cells J. Catal. Today 2004;90:277-81.

[57] Zhao L, Wang ZB, Sui XL, Yin GP. Effect of multiwalled carbon nanotubes with different specific surface areas on the stability of supported Pt catalyst. J. Power Sources 2014;245:637-43.

[58] Lin R, Zhang H, Zhao T, Cao C, Yang D, Ma J. Investigation of Au@Pt/C electro-catalysts for oxygen reduction reaction. Eletrochim Acta 2012;62:263-8.

[59] Katsounaros I, Schneider WB, Meier JC, Benedikt U, Biedermann PU, Auera AA, Mayrhofer KJJ. Hydrogen peroxide electrochemistry on platinum: towards understanding the oxygen reduction reaction mechanism. Phys. Chem. Chem. Phys. 2012;14:7384-91.

[60] Selvarani G, Vinod Selvaganesh S, Sridhar P, Pitchumani S, Shukla AK. Pt–Au/C cathode with enhanced oxygen-reduction activity in PEFCs. Bull. Mater. Sci. 2011;34:337-46.

[61] Antolini E, Giorgi L, Pozio A, Passalacqua E. Influence of Nafion loading in the catalyst layer of gas-diffusion electrodes for PEFC. J. Power Sources 1999;77:136-42.

[62] Watanabe M, Igarashi H, Yosioka K. An Experimental Prediction of the Preparation Condition of Nafion-Coated Catalyst Layers for PEFCs. Electrochim. Acta 1995;40:329-34.

[63] Poltarzewski Z; Staiti P, Alderucci V, Wieczorek W, Giordano N. Nafion Distribution in Gas Diffusion Electrodes for Solid-Polymer-Electrolyte-Fuel-Cell Applications. J. Electrochem. Soc. 1992;139:761-5.

[64] Uchida M, Aoyama Y, Eda N, Ohta A. Investigation of the Microstructure in the Catalyst Layer and Effects of Both Perfluorosulfonate Ionomer and PTFE-Loaded Carbon on the Catalyst Layer of Polymer Electrolyte Fuel Cells. J. Electrochem. Soc. 1995;142:4143-9.

[65] Passalacqua E, Lufrano F, Squadrito G, Patti A, Giorgi L. Nafion content in the catalyst layer of polymer electrolyte fuel cells: effects on structure and performance. Electrochim. Acta 2001;46:799-805.

Currículum vítae

José Roberto Flores Hernández
[*jrflores@iie.org.mx*]

Doctor en Electroquímica por la Albert-Ludwigs-Universität Freiburg I. Br., Alemania. Maestro en Ciencias en Química con especialidad en Electroquímica por el Tecnológico de Tijuana. Ingeniero Químico por la Benemérita Universidad Autónoma de Puebla (BUAP). Ingresó al Instituto de Investigaciones Eléctricas (IIE) en 1990 a la Gerencia de Energías Renovables de la División de Energías Alternas. Su área de especialidad se relaciona con la producción de hidrógeno vía la electrólisis del agua, donde ha diseñado y fabricado un prototipo industrial de *stack* de electrólisis, el cual ha pasado la fase de pruebas con un buen desempeño. Su actividad principal se enfoca en la fabricación de Ensambles Membrana-Electrodos (MEAs) para la tecnología de celdas de combustibles y electrolizadores. Ha realizado el desarrollo tecnológico del proceso de deposición automática de tinta catalítica para la fabricación de MEAs. Actualmente trabaja en la fabricación de MEAs para *stacks* de celdas de combustibles y la aplicación de las diferentes tecnologías de baterías en el área del almacenamiento de energía. Es autor de varios artículos nacionales e internacionales, así como de 3 patentes otorgadas, una en trámite y coautor de dos solicitudes de diseño industrial. Es miembro de la Sociedad Mexicana del Hidrógeno y de la Red de Energía Solar.

Tatiana Romero Castañón
[*tromero@iie.org.mx*]

Doctora con especialidad en Celdas de Combustible por la Universidad de British Columbia, Canadá. Maestra en Energía con mención honorífica por la Universidad Nacional Autónoma de México (UNAM). Ingeniera Química por la Universidad Popular Autónoma del Estado de Puebla (UPAEP). Ingresó al Instituto de Investigaciones Eléctricas (IIE) en al año 2000 y actualmente está adscrita a la Gerencia de Energías Renovables. Desde 2009 pertenece al Sistema Nacional de Investigadores (SNI). Su actividad principal se enfoca al desarrollo de técnicas de caracterización electroquímicas y desarrollo de celdas de combustible con incorporación de nanomateriales. Colabora con la Gerencia de Control e Instrumentación en el desarrollo de un método de control de humidificación para celdas de combustible a base de ultrasonido. Ha coordinado proyectos de colaboración internacionales con Canadá y Brasil, y ha participado en las reuniones de la Agencia Internacional de Energía representando a México en la sección de celdas de combustible. Cuenta con publicaciones en revistas científicas, participación en congresos internacionales. Es autora de 2 patentes otorgadas y coautora de dos solicitudes de diseño industrial.

Irma Lorena Albarrán Sánchez
[*ilas@iie.org.mx*]

Maestra en Ciencias por el Instituto de Ciencia y Tecnología de la Universidad de Manchester, Inglaterra, con especialidad en Procesos de Separación de Partículas. Ingeniera Química por la Universidad Autónoma del Estado de Morelos (UAEM), cuya tesis, desarrollada en el Instituto de Investigaciones Eléctricas (IIE), obtuvo el 2° Lugar del V Concurso Nacional de Tesis CONACYT-CFE-IIE. Ingresó al Departamento de Materiales del IIE en 1991, colaborando en el desarrollo de materiales poliméricos. Reingresó al IIE en 1994, a la hoy Gerencia de Procesos Térmicos, colaborando en la caracterización de fichas de atomización para centrales termoeléctricas mediante técnicas de difractometría láser. Actualmente trabaja en la Gerencia de Energías Renovables, en el desarrollo de tecnología de ensambles membrana-electrodos para celdas de combustible tipo PEM y Electrolizadores tipo PEM. Tiene diversas publicaciones en revistas nacionales e internacionales, es coautora de 3 patentes otorgadas, una en trámite y coautora de dos solicitudes de diseño industrial.
Es miembro de la Sociedad Mexicana de Hidrógeno.